SANDIA REPORT
SAND2008-6357
Unlimited Release
Printed September 2008

Hyperspectral Imaging of Oil Producing Microalgae under Thermal and Nutritional Stress

Mark H. Van Benthem, Amy J. Powell, Ryan W. Davis, J. Bryce Ricken, Todd W. Lane, Pamela Lane, and Michael R. Keenan

Prepared by
Sandia National Laboratories
Albuquerque, New Mexico 87185 and Livermore, California 94550

Sandia is a multiprogram laboratory operated by Sandia Corporation, a Lockheed Martin Company, for the United States Department of Energy's National Nuclear Security Administration under Contract DE-AC04-94AL85000.

Issued by Sandia National Laboratories, operated for the United States Department of Energy by Sandia Corporation.

Available to DOE and DOE contractors from
U.S. Department of Energy
Office of Scientific and Technical Information
P.O. Box 62
Oak Ridge, TN 37831

Telephone: (865) 576-8401
Facsimile: (865) 576-5728
E-Mail: reports@adonis.osti.gov
Online ordering: http://www.osti.gov/bridge

Available to the public from
U.S. Department of Commerce
National Technical Information Service
5285 Port Royal Rd.
Springfield, VA 22161

Telephone: (800) 553-6847
Facsimile: (703) 605-6900
E-Mail: orders@ntis.fedworld.gov
Online order: http://www.ntis.gov/help/ordermethods.asp?loc=7-4-0#online

SAND2008-6357
Unlimited Release
Printed September 2008

Hyperspectral Imaging of Oil Producing Microalgae under Thermal and Nutritional Stress

Mark H. Van Benthem and Michael R. Keenan
Materials Characterization Department
Amy J. Powell
Computational Systems Biology Department
Ryan W. Davis
Microsystem Materials Department
J. Bryce Ricken
Biomolecular Analysis & Imaging Department
Todd W. Lane and Pamela Lane
Biosystems Research Department
Sandia National Laboratories
P.O. Box 5800
Albuquerque, New Mexico 87185-0886

Abstract

This short-term, late-start LDRD examined the effects of nutritional deprivation on the energy harvesting complex in microalgae. While the original experimental plan involved a much more detailed study of temperature and nutrition on the antenna system of a variety of TAG producing algae and their concomitant effects on oil production, time and fiscal constraints limited the scope of the study. This work was a joint effort between research teams at Sandia National Laboratories, New Mexico and California. Preliminary results indicate there is a photosystem response to silica starvation in diatoms that could impact the mechanisms for lipid accumulation.

ACKNOWLEDGMENTS

This work was funded by Sandia Laboratory Directed Research and Development Office. The authors would like to thank Michael B. Sinclair, David M. Haaland, Howland D.T. Jones, David K. Melgaard, and Christopher L. Stork of Sandia National Laboratories for the software that they have developed that has been used in some of the analyses reported here. The authors also thank Jerilyn A. Timlin of SNL for her technical and editorial comments on this report. Sandia is a multi-program laboratory operated by Sandia Corporation, a Lockheed Martin Company, for the United States Department of Energy's National Nuclear Security Administration under contract DE-AC04-94AL85000.

CONTENTS

1. Introduction 7
   1.1. Algae Selection and Procurement 7
      1.1.1. Green Algae - Chlorophyta 8
      1.1.2. Diatoms 8
   1.2. Algae Culture 8
   1.3. Hyperspectral Imaging Confocal Microscopy 8
   1.4. Trilinear Data Analysis 9
2. Methods and Experimental 12
   2.1. Diatom Culture and Preparation 12
   2.2. HSI-CM Imaging 13
   2.3. Data Processing and Analysis 13
3. Results 15
4. Conclusions 22
5. References 23
Distribution 27

FIGURES

Figure 1. Rank estimate using eigenvalues of HSI-CM superimage. 15
Figure 2. PARAFAC analysis of nutritive-normal log-phase diatoms. 16
Figure 3. PARAFAC analysis of nutritive-normal log-phase diatoms with Nile Red. 17
Figure 4. PARAFAC analysis of Silica-Deprived (1) diatoms. 18
Figure 5. PARAFAC analysis of Silica-Deprived (1) diatoms with Nile Red. 19
Figure 6. PARAFAC analysis of Silica-Deprived (2) diatoms. 20
Figure 7. PARAFAC analysis of Silica-Deprived (2) diatoms with Nile Red. 21

TABLES

Table 1: Strains and species used in hyperspectral imaging studies (HSI) of algae under physiological stress 11

NOMENCLATURE

ALS	alternating least squares
CCD	charge couple device
chl a	chlorophyll *a*
chl c	chlorophyll *c*
DOE	Department of Energy
EMCCD	electron multiplying gain CCD
ESAW	artificial sea water medium
FOV	field of view
HSI-CM	hyperspectral imaging confocal microscope
MCR	multivariate curve resolution
PARAFAC	parallel factors analysis
PCA	principal component analysis
PE	phycoerythrin
PS II	photosystem two
RT	room temperature
SNL	Sandia National Laboratories
TAG	triacylglycerols
UTEX	University of Texas at Austin

1. INTRODUCTION

Production of oils from vegetation has the combined ability to reduce the nation's dependence on foreign sources of petroleum and decrease generation of CO_2. One of the most promising sources of natural oils, principally as triglycerides or triacylglycerols (TAGs), is microalgae.[1] The National Renewable Energy Laboratory spent nearly twenty years conducting the Aquatic Species Program, in which they investigated farming of microalgae.[2] One of their sites near Roswell, NM, demonstrated algae growth in open, stirred ponds. In attempts to generate high yields of oil, one of the most significant challenges they faced was the variability of ambient temperature. As the seasonal temperatures declined during the fall and further into winter, oil yields decreased, even when they changed crops to a more cold-resistant species. The fundamental conclusion from the work at Roswell was that temperature was the limiting factor in open pond algal-oil farming. One alternative to open pond systems is bioreactors. Bioreactors can be more productive than open pond systems, but have much higher capital costs associated with operations.[1]

The economics surrounding algal-oil production are somewhat complex. Considering the end use of algal-oil as biodiesel, it is a low value product which must be produced at low cost to be economically competitive. Open ponds have the potential advantage over bioreactors of lower capital costs, but typically have lower yields. Thus, the question of which method will prove economically viable remains open. As such, understanding algal growth and triglyceride production in outdoor pond-type-facilities is essential if one expects a commercial venture producing low-value biodiesel in sufficient quantities to satisfy national needs.

Given that the principal challenge associated with open pond growth is the effect of temperature, one of the original goals for this research effort was to investigate the effects of thermal stress on the energy harvesting and production of oil in algal species. Specifically, we planned to address the effects of temperature reduction on the energy collection system in algal species that show promise as producers of biodiesel feedstock. In addition, we intended to evaluate the effect of nutritional stresses on the energy collection system of these algal species. However, due to time constraints we limited the scope of the study.

While many studies have examined the spectroscopy and kinetics of the antenna molecules and reaction centers in microalgae,[3-7] few if any have examined them spatially within the organisms. Most examined them in bulk or as extracted from the organism. Our unique capabilities to collect confocal microscopic hyperspectral images,[8] combined with our state of the art data analysis algorithms allow us to bridge this knowledge gap. In the short operating period of this LDRD (approximately four months), we focused on a four basic tasks: 1) algae procurement, 2) algae culture, 3) hyperspectral imaging of algae and 4) multivariate data analysis.

1.1. Algae Selection and Procurement

Researchers estimate the number of species of green algae (Chlorophyta) and diatoms in the world at 14,000.[9, 10] Our interests are considerably limited to species that produce TAGs, are well-established in culture, and if possible, have had the genome mapped.

1.1.1. Green Algae - Chlorophyta

Nine different strains representing three species belonging to the taxonomic division Chlorophyta were employed in the present study (Table 1). One of these species, *Chlamydomonas reinhardtii*, is a well-established laboratory model that has recently had its genome fully sequenced.[11] *C. reinhardtii* is a flagellated, unicellular microalgae recognized as a model species for the study of photosynthesis.[11] During mitotic reproduction, *Chlamydomonas* loses its flagellum.[12] While *C. reinhardtii* does not accumulate lipids,[2] its value for research into energy harvesting is well-documented.

Another highly studied algal system is *Chlorella vulgaris*. *C. vulgaris* is a small unicellular microalgae and is not flagellated. It is used widely as a food additive[13] and herbal supplement,[14, 15] and is a producer of TAGs.[16, 17]

Botryococcus braunii has also been the focus of diverse research and development efforts, including those with bioenergy orientations, for a substantial period of time.[18]

1.1.2. Diatoms

Thalassiosira pseudonana is a model diatom species and has had its genome mapped by the Joint Genome Institute.[19] Diatoms are unicellular species that are renowned for their incorporation of silica in their cell walls. *T. pseudonana* is an oil producing autotrophic diatom.[20]

1.2. Algae Culture

Algae and diatoms would be cultured under standard laboratory conditions as controls.[21] In addition, modifications to media nutrients would allow evaluation of silica and nitrate availability in diatoms. In the case of green algae, experimental cultures would receive a one hour cold pulse at two temperatures (5°C or 10°C). Cells from control and experimental cultures would then be immediately prepared for imaging analyses.

1.3. Hyperspectral Imaging Confocal Microscopy

Hyperspectral fluorescence microscopy produces information-rich multivariate data with a full spectrum at each image pixel. The benefits of multivariate data over univariate data are well-known.[22] For hyperspectral microscopy, one of the most important of these benefits is the ability to discriminate amongst different fluorophores in the sample. Sandia National Laboratories (SNL) has developed a high performance hyperspectral imaging confocal microscope (HSI-CM).[8] It can collect images in three spatial dimensions, simultaneously recording the emission spectrum from native or introduced fluorophores at a maximum rate of 8300 spectral per second over the range of 500 nm to 800 nm. In its normal operational mode, the Sandia HSI-CM [8] collects two-way data in images that are on the order of 208×204 pixels by 512 emission wavelength elements.

Two-way hyperspectral data have numerous advantages over univariate data.[22] Among the most important of these is the ability to utilize exploratory techniques such as multivariate curve resolution (MCR) to analyze the data.[23-26] MCR is an iterative constrained least squares technique that estimates the image-mode pure components given an estimate of the pure-

component spectra followed by a complementary estimation of the spectral pure components using the image-mode pure components. The process is continued until some convergence criterion is achieved. Key to this methodology is the use of constraints, such as nonnegativity and equality, to provide physically meaningful solutions.

Using a supplementary data acquisition mode, temporal photobleaching, the HSI-CM can generate three-way data. Three-way data have additional advantages over two-way data, perhaps most powerful is the potential to obtain rotationally unique decompositions.[27]

1.4. Trilinear Data Analysis

In its rudimentary data acquisition mode, the HSI-CM[8] collects notionally bilinear data. That is, for an *R*-component chemical system, the data follow the model

$$f_{ij} = \sum_{p=1}^{R} c_{pi} s_{pj} \tag{1}$$

where f_{ij} is the fluorescence intensity at pixel i and wavelength j, c_{pi} is the concentration, or relative amount of the p^{th} fluorophore at pixel i, and s_{pj} is the unit-concentration fluorescence response for the p^{th} flourophore at wavelength j. While bilinear data is rich in information content, its decomposition into pure component concentrations and spectra is complicated by a mathematical peculiarity known as the rotation problem. The rotation problem arises because any solution for the factors matrices representing concentrations and spectra, *i.e.*, **C** and **S**. Simply stated, one can construct any invertible transformation matrix, **T**, to operate on **C** and **S** producing an identical solution to the least-squares cost function. Thus, in a least squares sense

$$\mathbf{F} = \mathbf{C}\mathbf{S}^{\mathrm{T}} = \left(\mathbf{C}\mathbf{T}^{-1}\right)\left(\mathbf{T}\mathbf{S}^{\mathrm{T}}\right). \tag{2}$$

Often, we can get around the rotation problem using constraints such as nonnegativity and various equality and other constraints. However, there is no guarantee that the solution one obtains is the most accurate representation of the true underlying information. Fortunately, there exist data types and analysis methods that can overcome the rotation problem, even in the absence of constraints. Trilinear data and trilinear decomposition methods fall into this category. Since the HSI-CM allows us to add additional acquisition modes, such as temporal photobleaching, which can vary linearly as do the concentration and wavelength modes, producing information-rich, rotationally-unique trilinear data.

Trilinear data follow the model[28-33],

$$f_{ijk} = \sum_{p=1}^{R} c_{pi} s_{pj} t_{pk}, \tag{3}$$

where f_{ijk} is the f_{ij} measured at the k^{th} time interval (or excitation wavelength) and t_{pk} is the concentration-independent photodecomposition rate for fluorophore p evaluated at time interval (or excitation wavelength) k. The matrix or array representation of Eq. 3 is

$$\mathbb{F} = \otimes(\mathbf{C}, \mathbf{S}, \mathbf{T}), \qquad (5)$$

where the fancy $\mathbb{F}$ is now a three-way array and the operator $\otimes$ represents the triple product of the pure component factor matrices **C**, **S**, and **T**. The solutions to the factor matrices can be estimated in a number of ways involving iterative methods and direct methods. We have had success using an iterative method known as parallel factors analysis or PARAFAC, which uses an alternating least squares scheme similar to MCR. While MCR alternately estimates **C** given **S**, and then **S** given **C** until convergence; PARAFAC-ALS (alternating least squares) estimates **C** given **S** and **T**, then **S** given **C** and **T**, and finally **T** given **C** and **S**. This approach lends itself well to our established expertise and fast algorithms developed for use with MCR.

We have developed novel fast algorithms for analyzing large three-way data sets and have successfully applied them to HSI-CM photobleach data. [34, 35] We will use this same strategy to analyze photobleach data of microalgae and fixed diatoms.

Table 1: Strains and species used in hyperspectral imaging studies (HSI) of algae under physiological stress

Strain	Species	Description
CC-503 cw92 mt +	*Chlamydomonas reinhardtii*	**Source:** Original mutant isolated by D.R. Davies in the Ebersold/Levine 137C wild-type background (equivalent to CC-125); this strain from George Witman, 1978 **Comment:** This is a clean, easily scored cell-wall deficient mutant that has been used successfully as a recipient for transformation. This strain was used as the source of DNA for the genome sequencing project at JGI.
CC-125 wild type mt+ 137c	*Chlamydomonas reinhardtii*	**Comment:** This is the basic "137c" wild type strain originally from G.M. Smith, isolated in 1945 near Amherst MA, and is presumably equivalent to strain 11/32c of the Culture Centre of Algae and Protozoa. This particular strain was brought to Duke by N.W. Gillham in 1968 from Levine's laboratory at Harvard. CC-124 and CC-125 carry the nit1 and nit2 mutations, and cannot grow on nitrate as their sole N source. CC-125 carries the AGG1 (agg1+) allele for phototactic aggregation; see *The Chlamydomonas Sourcebook* [Harris (1989)], p. 215. Contrast CC-124, which has the agg1 allele at this locus. **Comment:** CC-125 is the background strain for many mutations, and is a good control for most purpose
CC-124 wild type mt- 137c	*Chlamydomonas reinhardtii*	
UTEX Number: 26	*Chlorella vulgaris*	
UTEX Number: 30	*Chlorella vulgaris*	
UTEX Number: 2714	*Chlorella vulgaris*	
UTEX Number: 259	*Chlorella vulgaris*	
UTEX Number: 2441	*Botryococcus braunii*	
UTEX Number: 572	*Botryococcus braunii*	

2. METHODS AND EXPERIMENTAL

2.1. Diatom Culture and Preparation

T. pseudonana 3H (CCMP1335) was obtained from the Provasoli-Guillard Center for the Culture of Marine Phytoplankton at Bigelow Laboratory for Ocean Sciences (West Boothbay Harbor, MA). Cultures were maintained in ESAW medium (artificial sea water medium) under constant light 1000 µE and 21 °C. Cell numbers were determined by direct counting using a Coulter Z2 particle counter (Beckman Coulter Inc, Fullerton, CA). Experimental cultures were inoculated (2×10^4 cells-mL^{-1}) from mid logarithmic phase cultures that had been maintained for at least 3 passages under the same nutrient conditions as the experimental cultures. For silicate limited cultures standard ESAW was used (105 µM $NaSiO_3$). For nitrate limited cultures of the concentration of nitrate was lowered in ESAW from 549 µM to 50 µM and the silicate was doubled (210 µM $NaSiO_3$). Samples were taken at various time points and analyzed for TAGs by staining with Nile Red. All samples were normalized to 500,000-mL^{-1} for Nile Red staining and for fixation. Cells (with and without Nile Red) were fixed with 4% paraformaldehyde, washed and resuspended in ESAW. Protocols for Nile Red assay and paraformaldehyde fixation are below.

Each fixed diatom preparation contains 5×10^6 cells. The unstained samples were treated as follows: Cells were filtered using a suction pressure of less than 5" Hg onto 3µm, 25mm polycarbonate filter. Cells were then resuspended in 0.5 mL of cold 4% paraformaldehyde in a solution of 300 µL ESAW* and 200 µl 10% paraformaldehyde. ESAW* is prepared using ESAW plus an addition of 250mM NaCl to maintain salt concentration at approximately 0.4 M when mixed with paraformaldehyde. Cells were allowed to incubate on ice for 30 minutes. With vacuum off, 10 mL of cold ESAW was added to a funnel into which were subsequently added the fixed cells. The mixture was filtered using a suction pressure of less than 5" Hg. The filter was then washed four times with 10 mL aliquots of ESAW. Cells were finally resuspended in 0.5 mL ESAW and stored at 4ºC in the dark.

Nile Red dissolved in acetone (250 µg-mL^{-1}) was added to final concentration of 1 µg-mL^{-1} to 2 mL of cells (500,000 cells-mL^{-1}). The samples were allowed to incubate in the presence of the dye at room temperature (RT), for 150 seconds and subsequently excited at 530 nm while the fluorescent emission was measured from 550 nm to 750 nm.

The stained samples were treated as follows: 40 µl of 250 µg-mL^{-1} Nile Red solution was added to 10 mL of cells and then incubated at RT for 2.5 minutes. The cells were then treated identically to the unstained sample protocol described above.

Cultured *T. pseudonana* cells were harvested and fixed during mid logarithmic (day 2) late logarithmic (day 4) and stationary (day 10) phases of growth. Unstarved samples were derived from mid-lograrithmic phase cultures. As cultures deplete limiting nutrients they become starved for that nutrient and enter stationary phase. In the case of nitrate and silicate starvation, triacylglyceride accumulation initiates in stationary phase. Sample were stained, if necessary, fixed and shipped from SNL, CA to SNL, NM where they were imaged. Upon receipt and as permitted by schedule, these cells were imaged using the SNL HSI-CM.

2.2. HSI-CM Imaging

Confocal imaging of living and fixed algae samples in aqueous media was performed using the HSI-CM.[8] In these studies, repetitive exposure of cells resulted in differential bleaching of both endogenous and exogenous chromophores. Bleach series imaging and confocal sectioning was performed by rastering the instrument's 488 nm laser source over the 12.5 μm×12.5 μm fields of view (FOV) using a 60×, 1.4 NA Plan Apo objective (Nikon, Inc). The excitation power of the laser was maintained at 1.5 mW-μm^{-2} using neutral density filters. A neutral density emission filter was used to enable high bleaching intensity while preventing detector nonlinearities. Poly-l-lysine coated sample slides were used to immobilize diatom samples over the course of a multi-image bleach series. Eighteen measurements were made for each photobleached FOV. Spectral resolution of less than 3 nm over a 500 nm to 800 nm wavelength range was achieved using a custom readout mode of an electron multiplying gain CCD (EMCCD) camera (Andor) at a rate of 4000 spectra-sec^{-1}. Spatial resolution under these conditions is approximately 0.2 μm in the XY plane and 0.5 μm in the Z direction. Emission wavelength calibration was accomplished using a hollow-cathode Kr-ion lamp. "Dark" images were collected at regular intervals to provide an estimate of instrument offset and background signals. Image sizes were 104×100 pixels. Each diffraction limited region (~3 × 3 spatial pixels) illuminated for a 250 μsec exposure time per image.

2.3. Data Processing and Analysis

All data processing and analysis were performed using SNL authored programs written in MATLAB®[36] m-file language. All computations were performed using Dell Precision 690 equipped with two, dual-core, 3.2 GHz Xeon processors and 4.0 Gbyte RAM; operating under Windows XP Professional Version 2; and running MATLAB® version 7.6.0.324 (R2008a).

Data pretreatment included removing cosmic ray-induced spikes with an automated routine written in-house. The first six elements of the 512 element spectral mode were deleted to remove recurring noise artifacts. Each image was corrected for the wavelength dependent spectral response of the EMCCD by subtracting a rank-1 principal component analysis (PCA) estimate of the measured "dark" image. Next, a simple offset of typically a few counts or less was subtracted from each spectrum. The offset was estimated from a subset of the first 20 spectral elements, where an optical long-pass filter blocked any scatter or emission. Noise variance estimates of the Poisson-like noise were obtained using the mean in each data mode. The means were then multiplied by the EMCCD gain factor to correct for the amplification of the Poisson-noise variance due to the gain of the detector and a small noise amplification factor.[37, 38] An estimate of EMCCD read noise was obtained from the residual of the "dark" image after removal of its rank-1 PCA estimate The total noise variance in the data was then obtained by summing the gain-inflated means and the read noise variances.[37, 38] Data were compressed using a binning routine developed at SNL,[35] the data were then scaled by the inverse of the square-root of the total noise variances in each of the three modes[38, 39]. Rigorous nonnegativity constrained PARAFAC-ALS was performed on each three-way 130×506×18 binned image. Note that the first dimension here is the image-mode, whose 13×10 pixels are unfolded into a single variable since there is no implied interdependency by the least squares methods.

Compressed images were combined into a superimage using all FOVs collect on a sample. Rank analysis on images was performed using PCA of each mode of the superimage. PARAFAC analyses were initiated with previously obtained pure spectra component estimates from the previous rank estimates and/or random vectors as needed for the spectral, photobleach and image modes. Initial trilinear model estimate were obtained using a Fast Tucker1 PARAFAC-ALS algorithm[40] on the binned data. This was followed by PARAFAC on the binned data without PCA compression using an enhanced ALS algorithm that takes advantage of improvements in the formation of cross-products of data with the *Khatri-Rao* product.[40] After completing PARAFAC, the uncompressed data were projected into the space defined by the spectral and photobleach modes using a rigorous nonnegative least squares algorithm.

3. RESULTS

As part of our first challenge to the cultures of *T. pseudonana*, the cells were silica starved. Reduction of silica availability (starvation) is known to drive the production of TAGs in these diatoms. By reducing silica in the growth media in three stages we were able to monitor the effects on the energy harvesting system.

Figure 1 contains the eigenvalues from the superimage of the normally maintained (standard silica nutrition availability). Inspecting these scree plots, rank estimate is somewhat ambiguous and appears to be somewhere between 6 and 8. By comparison with rank-8 and higher decompositions, the rank-7 resolution presents a lower complexity solution and may be more interpretable. The solution to the rank-7 PARAFAC solution is displayed in Figure 2.

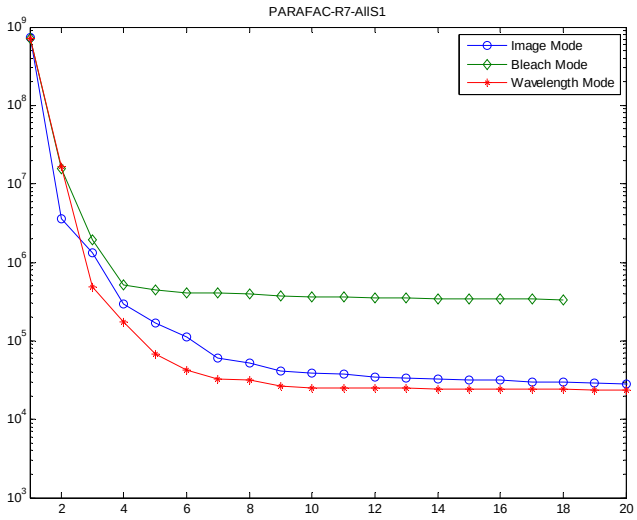

Figure 1. Rank estimate using eigenvalues of HSI-CM superimage.

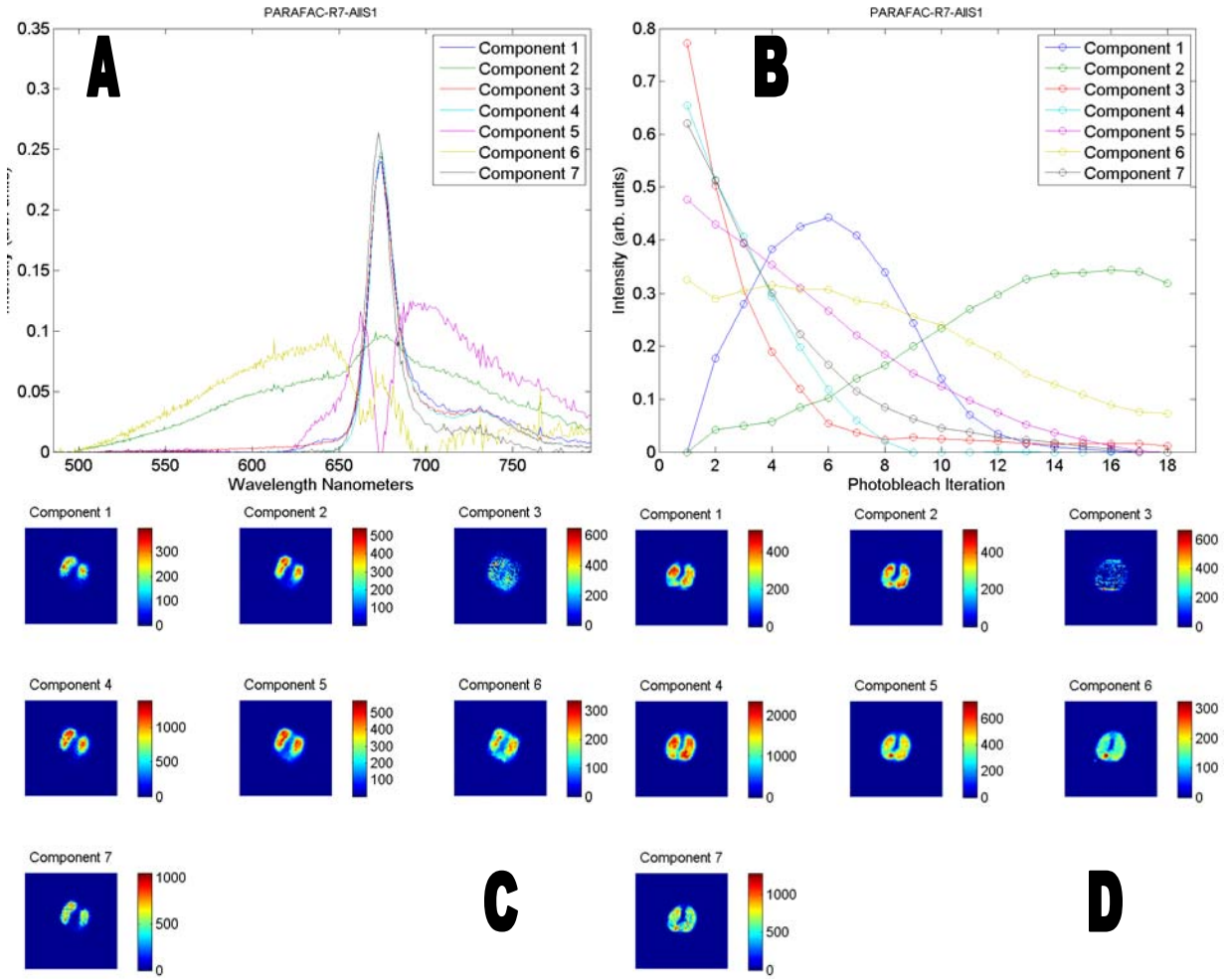

Figure 2. PARAFAC analysis of nutritive-normal log-phase diatoms.
Pure components analysis results for or seven factor PARAFAC model: A) spectral mode, B) bleach mode, C) image mode sample 3 of 5, and D) sample image mode 4 of 5 (other samples not shown).

Clearly the results of this analysis reveal a rather complex system of fluorophores and chromophores in these diatoms. The sharp peaks around 675 nm are chlorophyll(s) *a* (*chl a*)and part of photosystem (PS) II. The presence of so many *chl a* peaks can be interpreted as environmental effects of the *chl a* or an artifact-rich decomposition of the data. Component 1 peaks at 674 nm in the wavelength mode and behaves as an apparent intermediate form during the photobleaching process. Its initial intensity is close to zero and grows to a maximum at the sixth photobleach interval. It then proceeds to bleach completely before the last interval. Components 3, 4 and 7 all appear to exhibit first order bleaching kinetics. Component 6 is predominantly shorter wavelength emission and bleaches quite slowly. It also appears to have the weakest overlap with most of the *chl a* entities. Component 2 is the very broad emission which develops as a function of photobleaching. Component 5 is also a weak, very broad emission that is apparently slightly corrupted by *chl a*, which may be fucoxanthin.[41-43]

Figure 3 contains the PARAFAC results of the normal-silica nutrition medium, Nile Red-stained *T. pseudonana*.

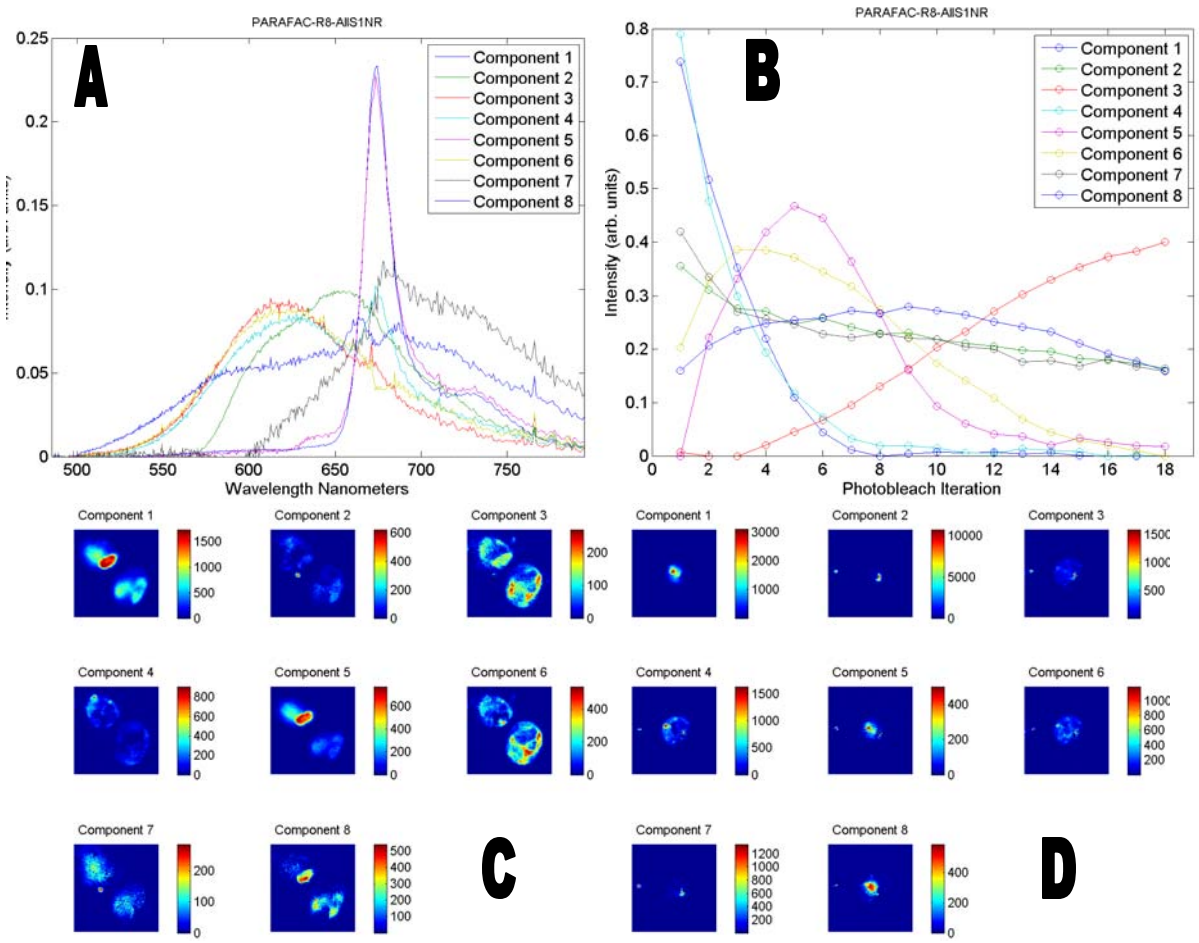

Figure 3. PARAFAC analysis of nutritive-normal log-phase diatoms with Nile Red.

Pure components analysis results for eight factor PARAFAC model: A) spectral mode, B) bleach mode, C) image mode sample 1 of 3, and D) image mode sample 2 of 3 (sample 3 not shown).

The results displayed above have a less complex *chl a* model compared to Figure 2. Here there are only two obvious components. Component 1 exhibits the first order decomposition, and Component 5 behaves as an intermediate species, cf. Component 1 above. Component 2 represents Nile Red. The dominant Nile Red signals are in very compact regions on the edge of or outside the cells. Components 3, 4 and 6 are heavily overlapped spectrally and represent one or several different pigments. These spectra peak around 615 nm and are in the spectral range of some phycobiliproteins, perhaps phycoerythrin (PE),[44] although these compounds are not normally found in diatoms. It is more likely that this component is chlorophyll c (*chl c*).[43, 45] However, the spatial distributions of these components are not highly colocalized with the *chl a* components, so it is unlikely they are involved in the light harvesting complex. Finally, again we see the weak, broad, long wavelength emission as Component 7 suspected to be fucoxanthin.

Figure 4 contains the eight-factor PARAFAC resolution of the silica-deprived *T. pseudonana*.

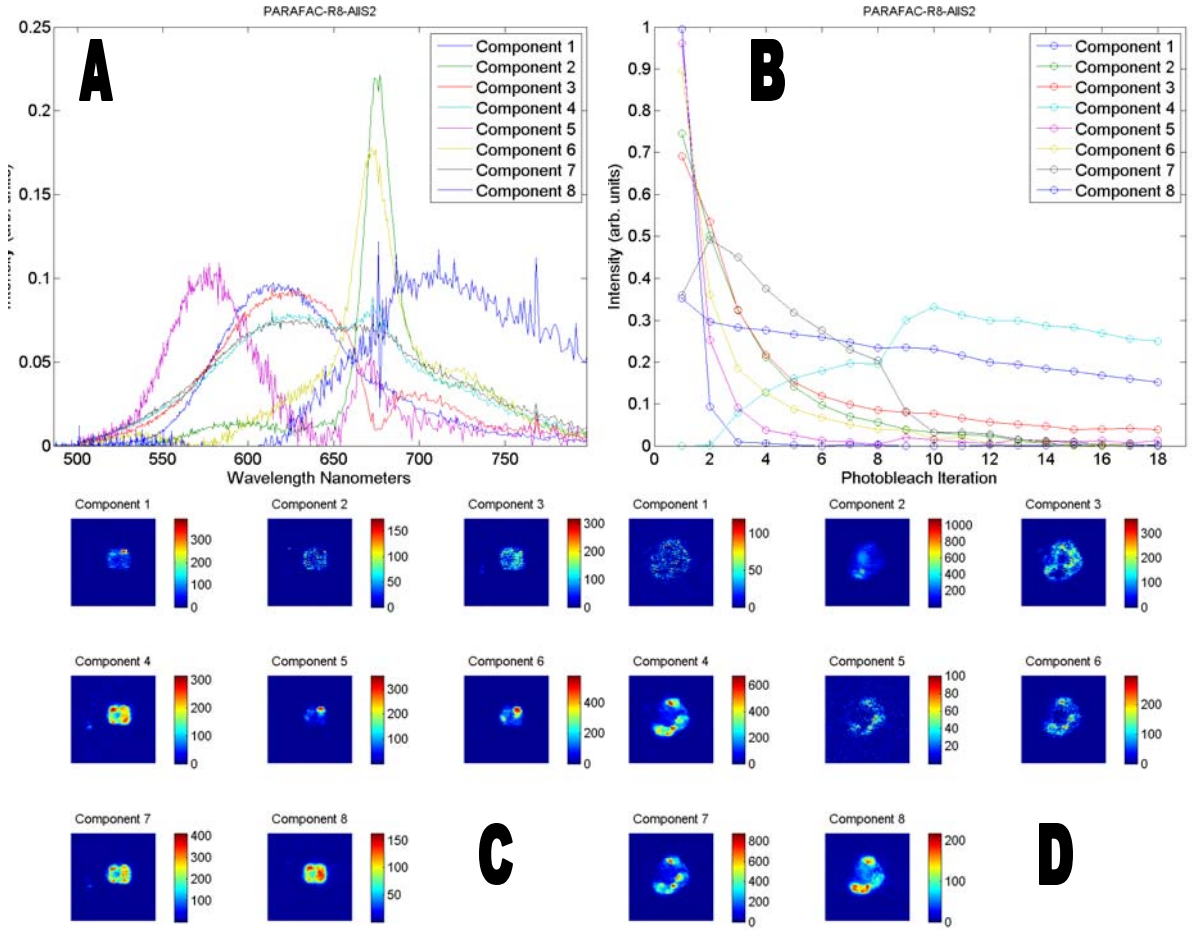

Figure 4. PARAFAC analysis of Silica-Deprived (1) diatoms.
Pure components analysis results for eight factor PARAFAC model: A) spectral mode, B) bleach mode, C) image mode sample 2 of 6, and D) image mode sample 4 of 6 (other samples not shown).

Inspecting the spectral-mode results in Figure 4 reveals a significant reduction in the complexity of the *chl a* fluorescence. In this case only Components 2 and 6 are associated with *chl a*. Both of these factors demonstrate first-order bleach behaviors, indicating loss of the intermediate form. Also evident in this resolution are the 615 nm peak factors (Components 1 and 3) tentatively identified as *chl c*. Once again they are not highly correlated with *chl a* in the spatial domain. Component 8 is the signal tentatively identified as fucoxanthin.

Figure 5 contains the seven-factor PARAFAC resolution of the silica-deprived *T. pseudonana* labeled with Nile Red.

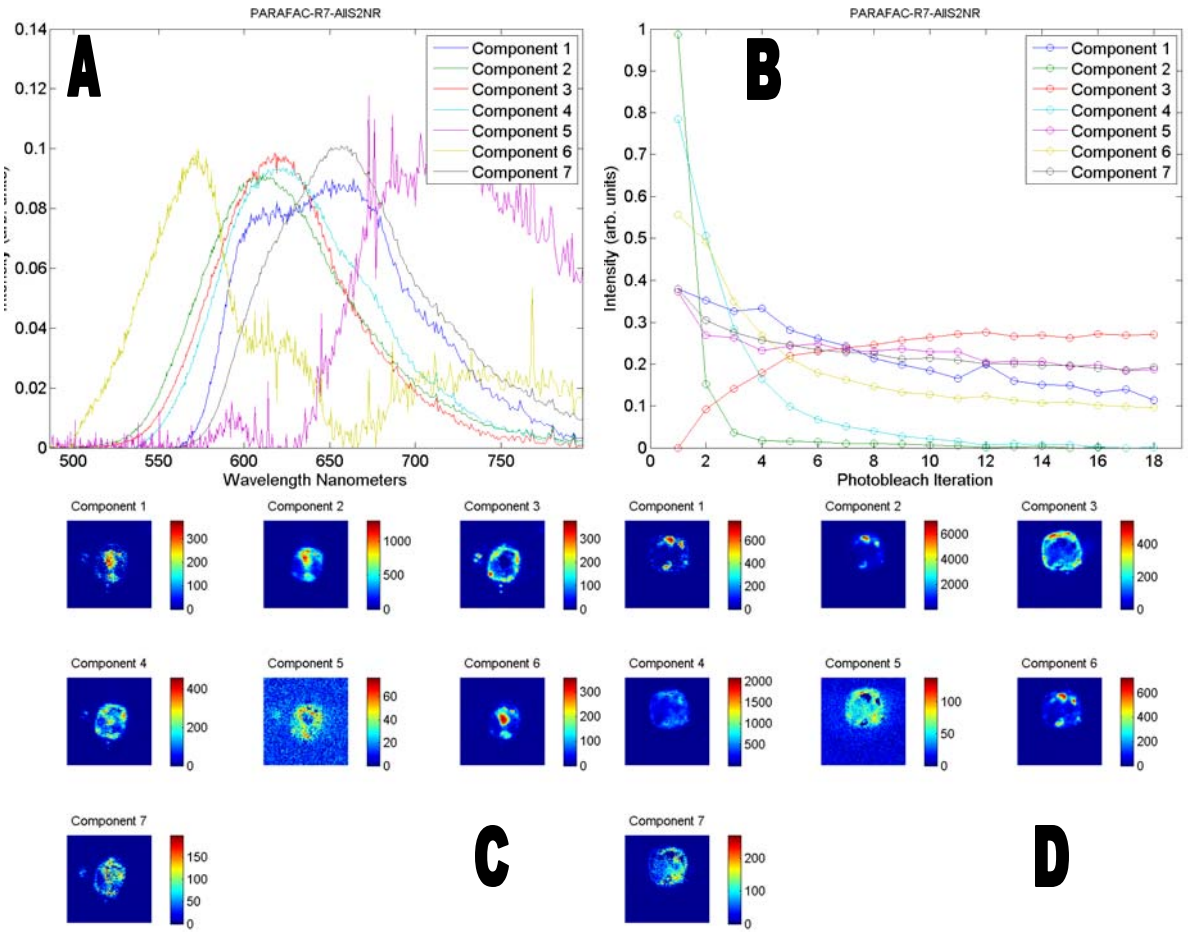

Figure 5. PARAFAC analysis of Silica-Deprived (1) diatoms with Nile Red.

Pure components analysis results for seven factor PARAFAC model: A) spectral mode, B) bleach mode, C) image mode sample 2 of 3, and D) image mode sample 3 of 3 (sample 1 not shown).

In these images, one can note that the peaks for *chl a* are missing. The factor representing Nile Red is Component 7. Under conditions of silica starvation, we find the TAGs labeled by Nile Red throughout the cell. The *chl c* peaks (Components 2, 3 and 4) also show distributions throughout the cell, although they are very distinct. Component 3 is found predominantly around the outer edge of the cell, while Component 4 is more-or-less evenly distributed in the cell.

Figure 6 contains the seven-factor PARAFAC resolution of the further silica-deprived *T. pseudonana*.

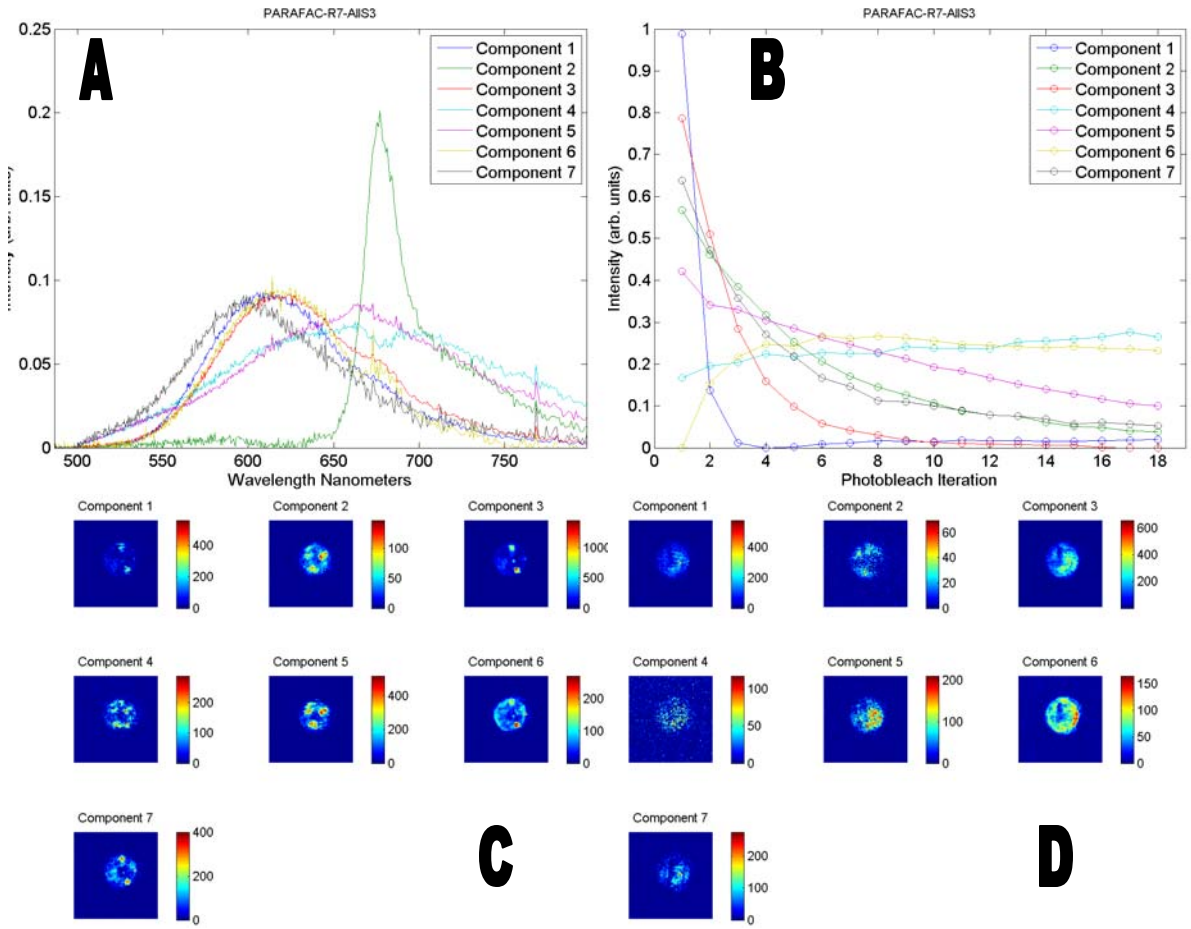

Figure 6. PARAFAC analysis of Silica-Deprived (2) diatoms.
Pure components analysis results for seven factor PARAFAC model: A) spectral mode, B) bleach mode, C) image mode sample 2 of 6, and D) image mode sample 5 of 6 (other samples not shown).

Here the *chl a* peak (Component 2) is poorly resolved and is very weak in its contribution to the overall fluorescence. On the other hand, the *chl c* peaks (Components 1, 3, 6 and 7) are once again found throughout the cells.

Figure 7 contains the seven-factor PARAFAC resolution of the further silica-deprived *T. pseudonana* labeled with Nile Red.

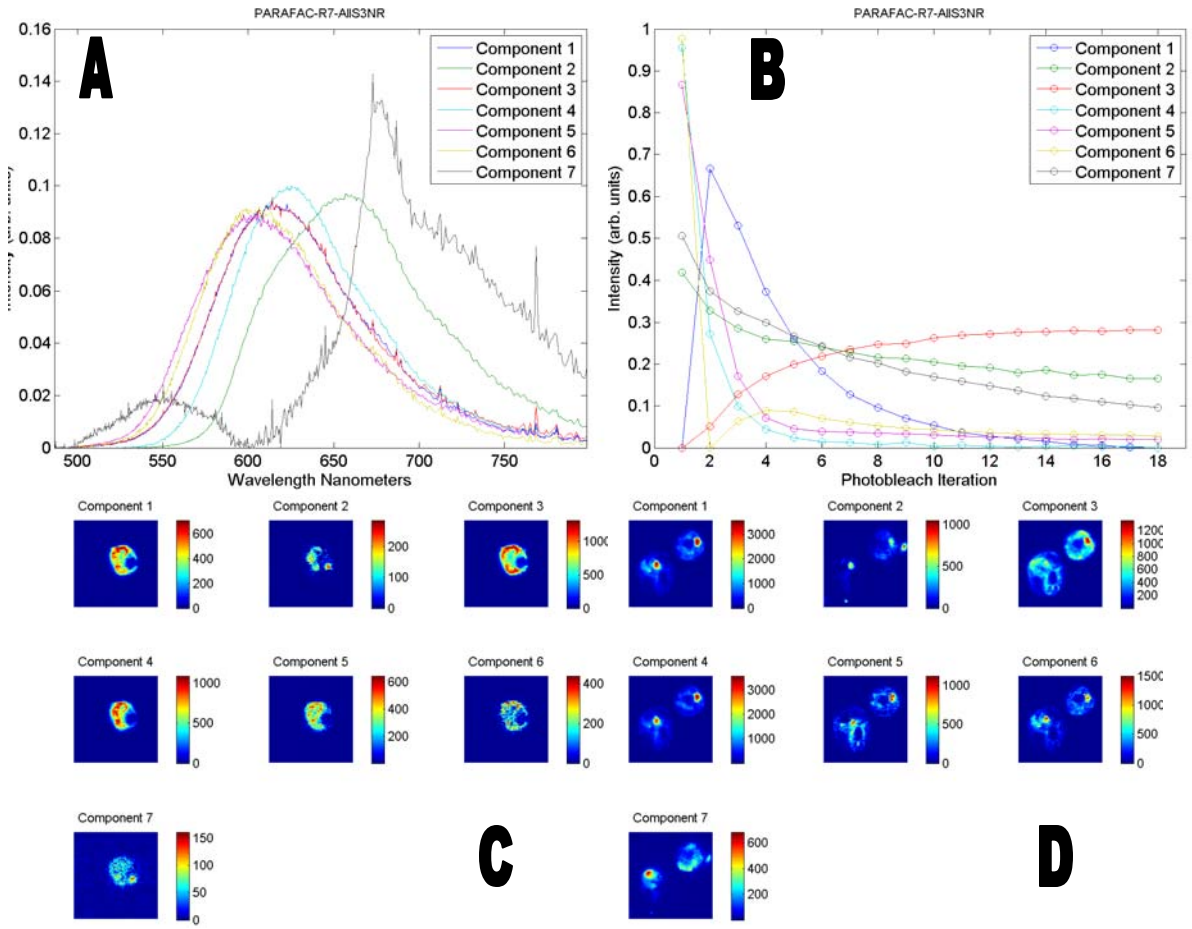

Figure 7. PARAFAC analysis of Silica-Deprived (2) diatoms with Nile Red.

Pure components analysis results for seven factor PARAFAC model: A) spectral mode, B) bleach mode, C) image mode sample 2 of 6, and D) image mode sample 4 of 6 (other samples not shown).

As we found immediately above, the *chl a* peak (Component 7) is poorly resolved and not significantly contributing to the fluorescence signal. The Nile Red (Component 2) is found to be highly localized inside and outside the cell. It does not appear to be in greater abundance than found in Figure 5. The *chl c* peaks (Components 1, 3, 4, 5 and 6) dominate the fluorescence.

4. CONCLUSIONS

This short-term, late-start LDRD examined the effects of nutritional deprivation on the energy harvesting complex in microalgae. While the original experimental plan involved a much more detailed study of temperature and nutrition on the antenna system of a variety of TAG producing algae and their concomitant effects on oil production, time and fiscal constraints limited the scope of the study.

We were able to cultivate a number of algae species and develop techniques for future studies. In addition, we were able to image the diatom *T. pseudonana* under nutritional stresses using unique SNL's HSI-CM. Our results, while limited and preliminary, indicate that the reduction of silica has the effect of reducing the fluorescence response of *chl a* in PS II for mild stresses. This phenomenon could be very important in understanding TAG production and accumulation and should be considered for further study.

5. REFERENCES

1. M. S. Kent and K. M. Andrews, "Biological Research Survey for the Efficient Conversion of Biomass to Biofuels," Sandia National Laboratories, Albuquerque, NM, SAND2006-7221, (2007).
2. J. Sheehan, T. Dunahay, J. Benemann and P. Roessler, "A Look Back at the U.S. Department of Energy's Aquatic Species Program—Biodiesel from Algae," National Renewable Energy Laboratory, Golden, CO, NREL/TP-580-24190, (1998).
3. O. Canaani and E. Gantt, "Formation Of Hybrid Phycobilisomes By Association Of Phycobiliproteins From Nostoc And Fremyella," *Proc. Natl. Acad. Sci. U. S. A.* **79**(17), 5277-5281 (1982)
4. T. G. Owens, *et al.*, "Antenna structure and excitation dynamics in photosystem I. I. Studies of detergent-isolated photosystem I preparations using time-resolved fluorescence analysis," *Biophys. J.* **53**(5), 733-745 (1988)
5. M. Mimuro, "Visualization of excitation energy transfer processes in plants and algae," *Photosynthesis Research* **73**(1/3), 133-138 (2002)
6. T. Polivka, *et al.*, "Energy transfer in the major intrinsic light-harvesting complex from Amphidinium carterae," *Biochemistry* **45**(28), 8516-8526 (2006)
7. T. Polivka, R. G. Hiller and H. A. Frank, "Spectroscopy of the peridinin-chlorophyll-a protein: Insight into light-harvesting strategy of marine algae," *Arch. Biochem. Biophys.* **458**(2), 111-120 (2007)
8. M. B. Sinclair, D. M. Haaland, J. A. Timlin and H. D. T. Jones, "Hyperspectral confocal microscope," *Appl. Opt.* **45**(24), 6283-6291 (2006)
9. A. D. Chapman, "Numbers of Living Species in Australia and the World," (2005) http://www.environment.gov.au/biodiversity/abrs/publications/other/species-numbers/03-04-groups-others.html, Date Accessed: 17 Sep 08
10. M. Guiry, "AlgaeBase — listing the world's algae," *in The Irish Scientist 2005 Yearbook* G. Van Esbeck, Ed., pp. 74-75, Oldbury Publishing Limited, Dublin, Ireland (2005).
11. S. S. Merchant, *et al.*, "The Chlamydomonas Genome Reveals the Evolution of Key Animal and Plant Functions," *Science* **318**(5848), 245-250 (2007)
12. E. W. Nester, *et al.*, *Microbiology*, Saunders College Publishing, Philadelphia, PA (1983).
13. A. Raymundo, *et al.*, "Fat mimetic capacity of Chlorella vulgaris biomass in oil-in-water food emulsions stabilized by pea protein," *Food Research International* **38**(8-9), 961-965 (2005)
14. G. C. Jagetia and M. S. Baliga, "Treatment of mice with a herbal preparation (Mentat) protects against radiation-induced mortality," *PHYTOTHERAPY RESEARCH* **17**(8), 876-881 (2003)
15. S. Liang, X. Liu, F. Chen and Z. Chen, "Current microalgal health food R & D activities in China," *Hydrobiologia* **512**(1), 45-48 (2004)
16. B. W. Nichols, A. T. James and J. Breuer, "Interrelationships between fatty acid biosynthesis and acyl-lipid synthesis in Chlorella vulgaris," *Biochem. J.* **104**(2), 486-496 (1967)
17. A. H. Scragg, J. Morrison and S. W. Shales, "The use of a fuel containing Chlorella vulgaris in a diesel engine," *Enzyme Microb. Technol.* **33**(7), 884-889 (2003)
18. P. Metzger and C. Largeau, "Botryococcus braunii: a rich source for hydrocarbons and related ether lipids," *Appl. Microbiol. Biotechnol.* **66**(5), 486-496 (2005)

19. E. V. Armbrust, *et al.*, "The Genome of the Diatom Thalassiosira Pseudonana: Ecology, Evolution, and Metabolism," *Science* **306**(5693), 79-86 (2004)
20. T. Tonon, *et al.*, "Fatty acid desaturases from the microalga *Thalassiosira pseudonana*," *FEBS Journal* **272**(13), 3401-3412 (2005)
21. D. T. Hanson, L. A. Franklin, G. Samuelsson and M. R. Badger, "The Chlamydomonas reinhardtii cia3 mutant lacking a thylakoid lumen-localized carbonic anhydrase is limited by CO2 supply to rubisco and not photosystem II function in vivo," *Plant Physiol.* **132**(4), 2267-2275 (2003)
22. K. S. Booksh and B. R. Kowalski, "Theory of analytical chemistry," *Anal. Chem.* **66**(15), A782-A791 (1994)
23. R. Tauler and D. Barcelo, "Multivariate curve resolution applied to liquid chromatography-diode array detection," *Trends Anal. Chem.* **12**(8), 319-327 (1993)
24. M. H. Van Benthem, M. R. Keenan and D. M. Haaland, "Application of equality constraints on variables during alternating least squares procedures," *J. Chemometrics* **16**(12), 613-622 (2002)
25. R. Tauler, "Multivariate Curve Resolution Applied to 2nd-Order Data," *Chemometrics Intell. Lab. Syst.* **30**(1), 133-146 (1995)
26. M. R. Keenan, J. A. Timlin, M. H. Van Benthem and D. M. Haaland, "Algorithms for constrained linear unmixing with application to the hyperspectral analysis of fluorophore mixtures," *in Imaging Spectrometry VIII* S. S. Shen, Ed., pp. 193-202, SPIE - The International Society for Optical Engineering, Seattle, WA, USA (2002).
27. R. A. Harshman, "Foundations of the PARAFAC procedure: Model and conditions for an 'explanatory' multi-mode factor analysis," *UCLA Working Papers Phonetics* **16**(1–84 (1970)
28. R. A. Harshman and M. E. Lundy, "Parafac : Parallel Factor-Analysis," *Computational Statistics & Data Analysis* **18**(1), 39-72 (1994)
29. R. Bro, "PARAFAC. Tutorial and applications," *Chemometrics Intell. Lab. Syst.* **38**(2), 149-171 (1997)
30. J. B. Kruskal, "Rank, Decomposition, and Uniqueness for 3-way and N-way Arrays," *in Multiway Data Analysis* R. Coppi and S. Bolasco, Eds., pp. 7-18, North-Holland, Amsterdam (1989).
31. B. C. Mitchell and D. S. Burdick, "Slowly Converging parafac sequences: Swamps and two-factor degeneracies," *J. Chemometrics* **8**(155-168 (1994)
32. S. E. Leurgans and R. T. Ross, "Multilinear models: Applications in spectroscopy," *Statistical Science* **7**(3), 289-319 (1992)
33. G. Tomasi and R. Bro, "A comparison of algorithms for fitting the PARAFAC model," *Computational Statistics & Data Analysis* **50**(7), 1700-1734 (2006)
34. M. H. Van Benthem and M. R. Keenan, "Tucker1 model algorithms for fast solutions to large PARAFAC problems," *J. Chemometrics* **22**(5), 345-354 (2008)
35. M. H. Van Benthem, *et al.*, "Trilinear Analysis Of Images Obtained With A Hyperspectral Imaging Confocal Microscope," *J. Chemometrics* (Published Online: Jul 9 2008)
36. "MATLAB," The MathWorks, Inc., Natick, MA (2008).
37. J.-L. Starck, F. D. Murtagh and A. Bijaoui, *Image Processing and Data Analysis: The Multiscale Approach*, Cambridge University Press, Cambridge, UK (1998).
38. H. D. T. Jones, *et al.*, "Weighting Hyperspectral Image Data for Improved Multivariate Curve Resolution Results," *J. Chemometrics* (submitted for publication)

39. M. R. Keenan and P. G. Kotula, "Accounting for Poisson noise in the multivariate analysis of ToF-SIMS spectrum images," *Surf. Interface Anal.* **36**(3), 203-212 (2004)
40. M. H. Van Benthem and M. R. Keenan, "Tucker1 Model Algorithms For Fast Solutions To Large PARAFAC Problems," *J. Chemometrics* (accepted for publication)
41. T. Katoh, U. Nagashima and M. Mimuro, "Fluorescence properties of the allenic carotenoid fucoxanthin: Implication for energy transfer in photosynthetic pigment systems," *Photosynthesis Research* **27**(3), 221-226 (1991)
42. A. L. Friedman and R. S. Alberte, "A Diatom Light-Harvesting Pigment-Protein Complex : Purification and Characterization," pp. 483-489 (1984).
43. E. Papagiannakis, *et al.*, "Spectroscopic characterization of the excitation energy transfer in the fucoxanthin-chlorophyll protein of diatoms," *Photosynthesis Research* **86**(1-2), 241-250 (2005)
44. J. Seppala and M. Balode, "The use of spectral fluorescence methods to detect changes in the phytoplankton community," *Hydrobiologia* **363**(207-217 (1998)
45. A. W. Larkum, *et al.*, "Light-harvesting chlorophyll c-like pigment in Prochloron," *Proc. Natl. Acad. Sci. U. S. A.* **91**(2), 679-683 (1994)

DISTRIBUTION

Electronic copy to:

1	MS0886	Mark Van Benthem	01822
1	MS1413	Amy Jo Powell	08333
1	MS1411	Ryan Davis	01824
1	MS9292	Todd Lane	08321
1	MS9671	Pamela Lane	08321
1	MS1413	Bryce Ricken	08332
1	MS0886	Michael Keenan	01822
1	MS0895	Tony Martino	08332
1	MS1413	Grant Heffelfinger	08330
1	MS0895	Jerilyn Timlin	08332
1	MS9292	Blake Simmons	08755

Hardcopy to:

2	MS9018	Central Technical Files	8944
2	MS0899	Technical Library	4536
1	MS0123	D. Chavez, LDRD Office	1011


Sandia National Laboratories